

Grinding-hardening with liquid nitrogen: Mechanisms and technology

T. Nguyen, I. Zarudi, L.C. Zhang*

School of Aerospace, Mechanical and Mechatronic Engineering, The University of Sydney, NSW 2006, Australia

Received 9 January 2006; accepted 17 February 2006

Available online 11 April 2006

Abstract

This paper studies an innovative development of a steel grinding-hardening technology using an inert cryogen—liquid nitrogen. It was found that phase transformations took place during grinding with the application of liquid nitrogen and resulted in hardened surface layer in a ground component. The layer had a fine laths martensite structure which gave rise to a remarkably high hardness. It was also shown that the treatment can produce superior surface integrity, with compressive surface residual stresses and without surface oxidation. Due to the inert nature of the liquid nitrogen, the grinding process becomes environmentally conscious.

© 2006 Elsevier Ltd. All rights reserved.

Keywords: Grinding liquid nitrogen; Microstructure; Residual stresses; Hardness; Phase transformation; Oxidation suppression

1. Introduction

Grinding-hardening treatment has attracted significant research attention worldwide due to its efficiency and unique properties of ground workpiece [1–7]. Relevant theoretical and experimental studies have shown clear advantages of grinding-hardening which combines surface heat treatment with surface finishing.

In the investigations on grinding-induced surface integrity in steel workpieces [8,9], it was found that phase transformations during surface grinding, which in turn resulted in hardening characteristics, could be achieved by a proper selection of grinding conditions. It was also found that the depth and property of the martensite layer and the distribution of residual stresses could be described quantitatively with respect to the material removal rate and coolant application method.

Experimental studies also reported that the grinding energy could be used to generate a hard surface [1,2,6]. However, a hardened layer does not necessarily mean beneficial, rather, it can be harmful if the layer is associated with a poor surface finish, uncontrollable precision, tensile

residual stresses, damaged microstructure or severe surface oxidation [5,6].

One way to eliminate these problems is by applying new types of coolant. It has been noticed that in the field of welding, oxidation is one of the major causes in weakening the strength of welds. To overcome the problem, nitrogen gas has been used in shielding the welding spot [10]. On the other hand, liquid nitrogen, because of its extremely low boiling temperature, has been widely applied in cryogenic treatment of tool steels to convert austenite retained from conventional quenching to a more rigid structure of martensite [11–16]. It is clear that liquid nitrogen whilst acts as a protective shielding, can also provide high cooling rates to promote metallurgical changes. However, these advantages have not been explored in grinding.

This paper proposes an innovative development of grinding-hardening technology using liquid nitrogen to integrate precision surface grinding with surface hardening treatment, and at the same time, to produce satisfactory surface integrity of ground components, including compressive surface residual stresses and fine microstructure with high hardness. Because of the inert nature of liquid nitrogen, the grinding process becomes environmentally conscious.

*Corresponding author. Tel.: +61 2 9351 2835; fax: +61 2 9351 7060.
E-mail address: zhang@aeromech.usyd.edu.au (L.C. Zhang).

Table 1
Chemical composition and mechanical properties of steel 1045

Chemical compositions, %				Mechanical properties		
C	Mn	P, max	S, max	Tensile strength (MPa)	Micro-hardness (HV _{0.5})	Yield strength (MPa)
0.42–0.50	0.60–0.90	0.040	0.050	630	172.9 ± 11.1	530

Table 2
Grinding and dressing conditions

Grinding machine	Minini Junior 90 CNC-M286
Workpiece	<ul style="list-style-type: none"> ● Plain carbon steel 1045, 45 × 19.5 × 19.5 mm ● Vacuumed pre-annealing at above 600 °C ● Initial surface residual stress: -10.00 ± 8.00 MPa (longitudinal) and -10.39 ± 8.00 MPa (transverse)
Grinding method	Surface up grinding
Grinding wheel	BWA60MVA1, $\phi 260 \times 20$
Dressing	<ul style="list-style-type: none"> ● Single point diamond ● Transverse rate = 160 $\mu\text{m}/\text{rev}$ ● Total dressing depth = $2 \times 25 \mu\text{m}$
Wheel speed	23 m/s
Table speed	400 mm/min
Depth of cut	20 μm
Cooling	Atmospheric dry air, ambient temperature = 20 °C
	Liquid nitrogen, $Q = 2.18$ L/min
	Noritake SA-02 (1:60), $Q = 18.8$ L/min

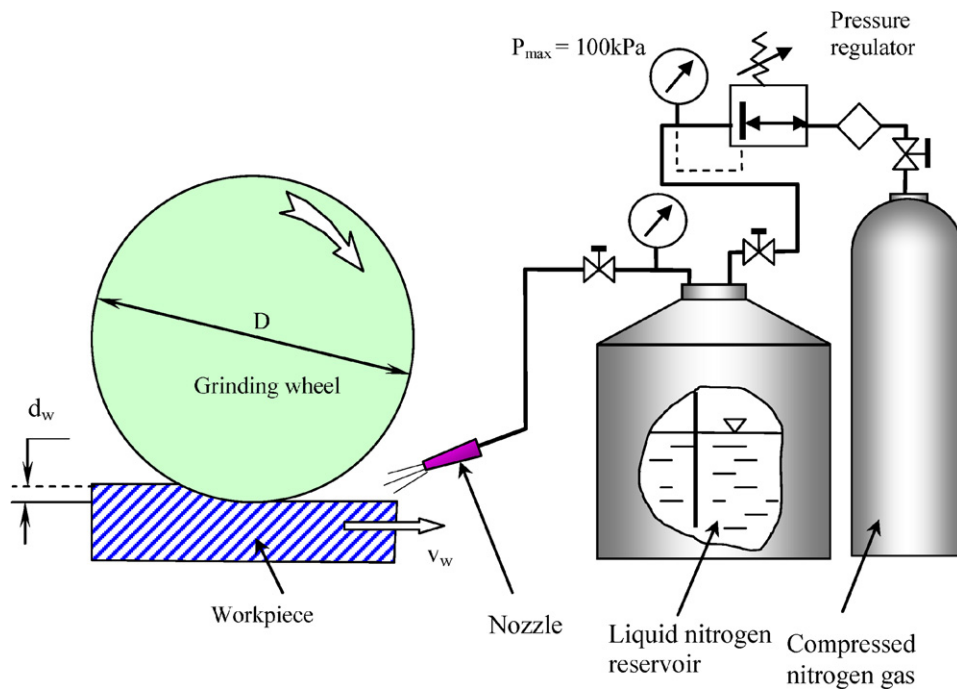


Fig. 1. The experimental set-up using liquid nitrogen.

2. Experiment

The test material was widely used steel, AISI 1045, initially annealed. The chemical composition of the steel is listed in Table 1. Grinding was performed on a surface

grinder, Minini Junior 90 CF CNC M286. The grinding and dressing conditions are listed in Table 2.

Fig. 1 shows the experimental set-up of surface grinding with liquid nitrogen. The internal pressure of the reservoir was 50 kPa, controlled by a regulator. A nozzle with the

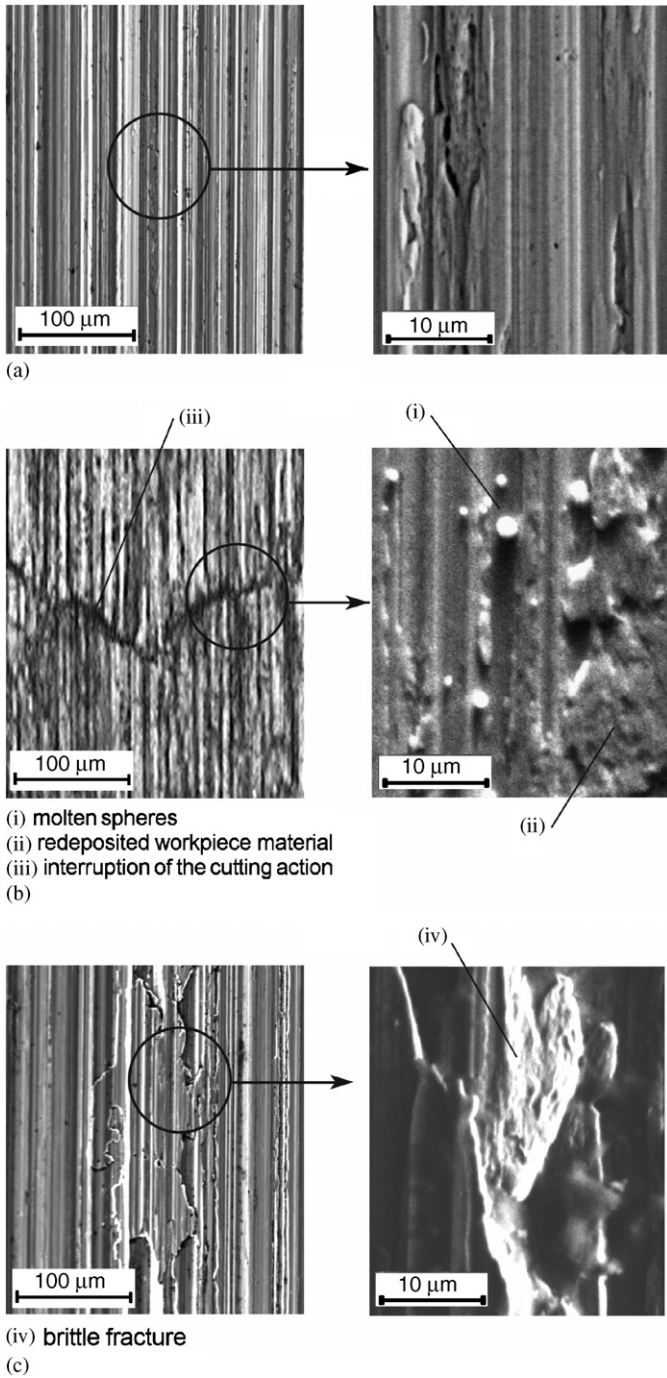


Fig. 2. The surface topography after grinding: (a) with coolant; (b) in the dry air; (c) with liquid nitrogen.

outlet diameter of 2 mm was mounted on the wheel guard to provide a liquid jet to the grinding point from a distance of 50 mm with an angle of 30° tangential to the specimen surface. Up-grinding was used to facilitate the penetration of liquid nitrogen into the grinding zone. After grinding, a ground workpiece was left in liquid nitrogen for 600 s, and then lifted to the ambient until its temperature reached room temperature.

The micro-hardness (HV) of the subsurface was examined on cross-section view samples with a hardness tester,

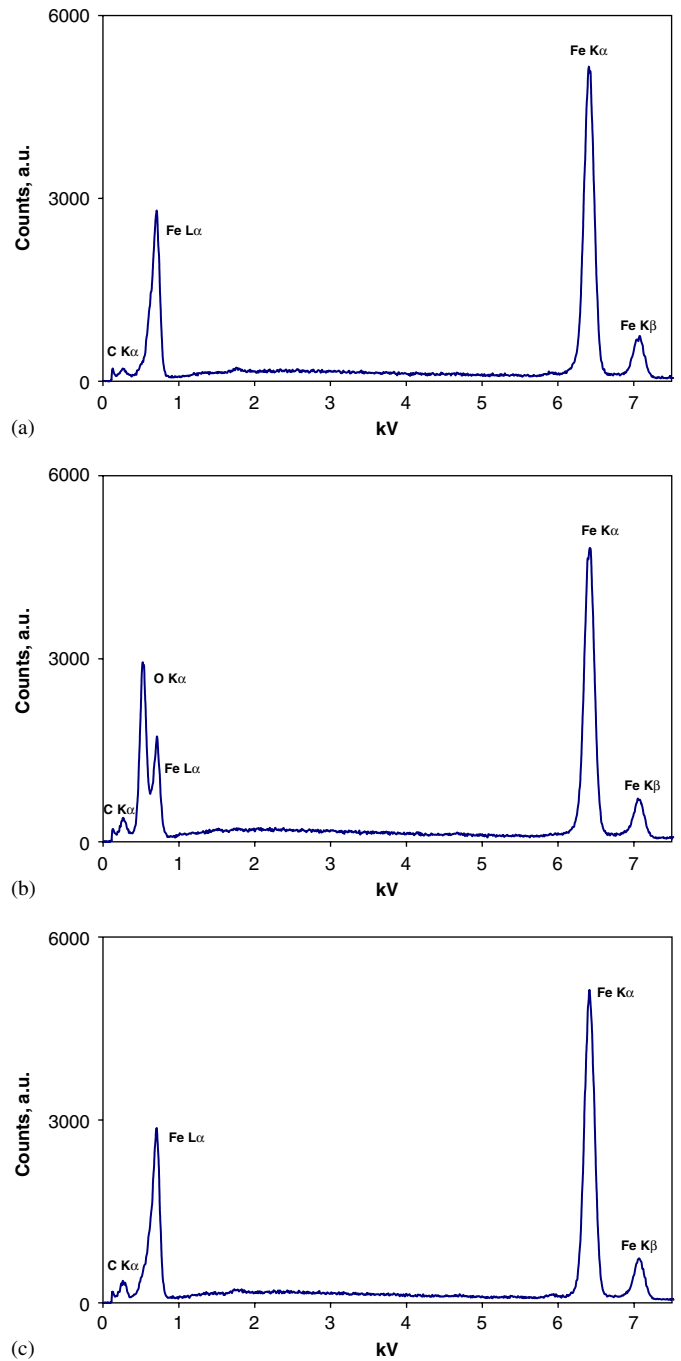


Fig. 3. EDX spectra from the ground surface after grinding: (a) with coolant; (b) in the dry air; (c) with liquid nitrogen.

Shimadzu Seisakusho, NT-M001. The topography of ground surfaces was observed on the scanning electron microscope (SEM), 505 (JEOL). Residual stresses in a ground specimen were measured on an X-ray diffraction machine, Rigaku MSF-3 M. The removal of the surface layers in the residual stress measurement was performed on an electro-polishing machine, Movipol-3. The thickness removed in each step was determined on an optical microscope, Leica DM RXE. The characterization of the electron structure of the ground surfaces was done on a

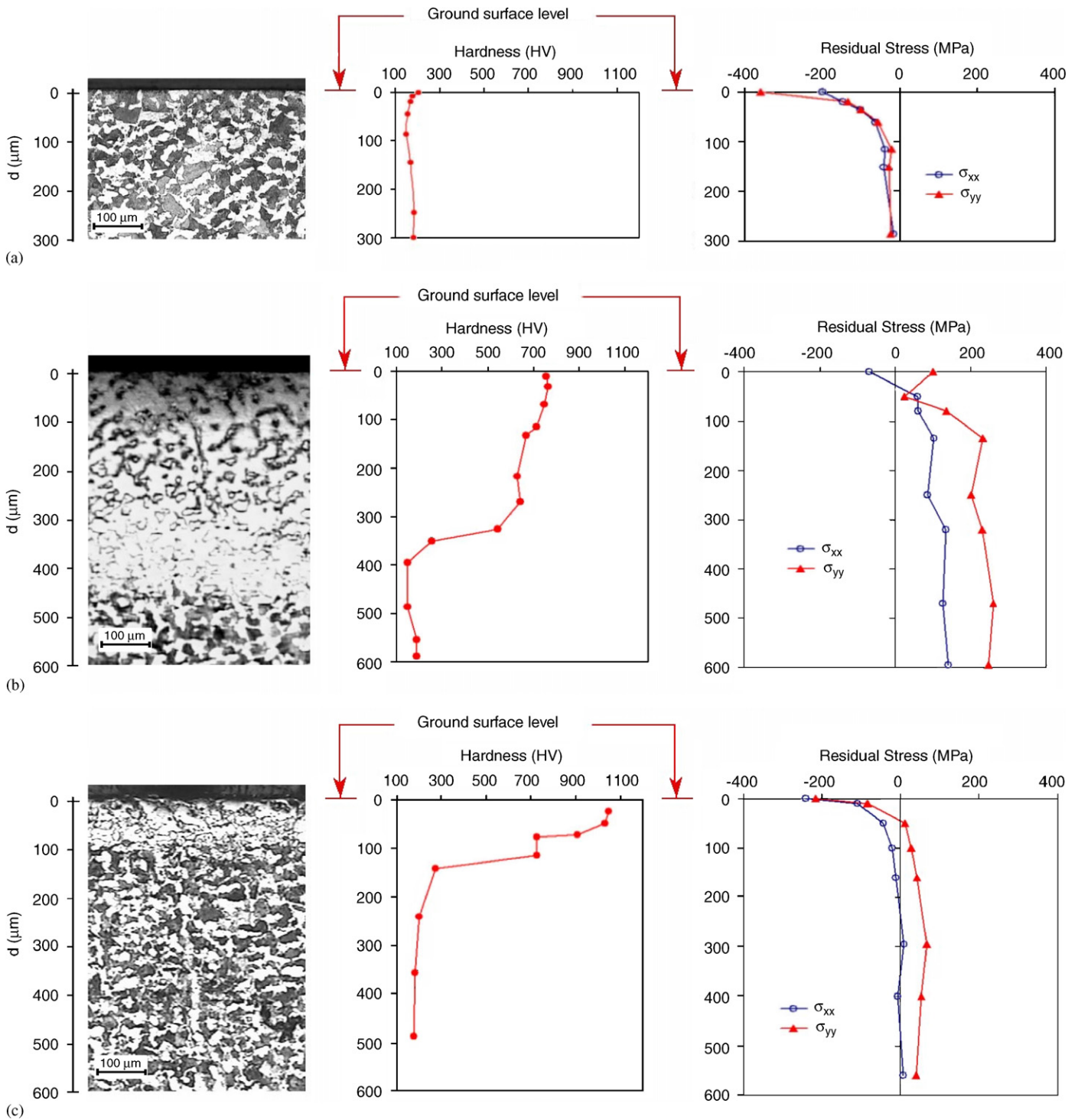


Fig. 4. Subsurface structure, hardness and residual stresses after grinding: (a) with coolant; (b) in the dry air; (c) with liquid nitrogen.

transmission electron microscope (TEM), CM12 (Philips). TEM plan view specimens were prepared in a standard manner using a tripod, whose thinning procedure was performed from the side opposite to ground surface. At the final stage, ion-beam thinning was used to achieve a sufficiently thin area for TEM. In sample preparation, the specimen temperature was kept below 40 °C to ensure that no microstructural changes would take place.

3. Results and discussion

3.1. Surface topography

Fig. 2 presents the surface topography of the ground surfaces after grinding with different cooling media.

Grinding with Noritake coolant (Fig. 2(a)) has generated continuous and shallow grooves with roughness (R_a) of

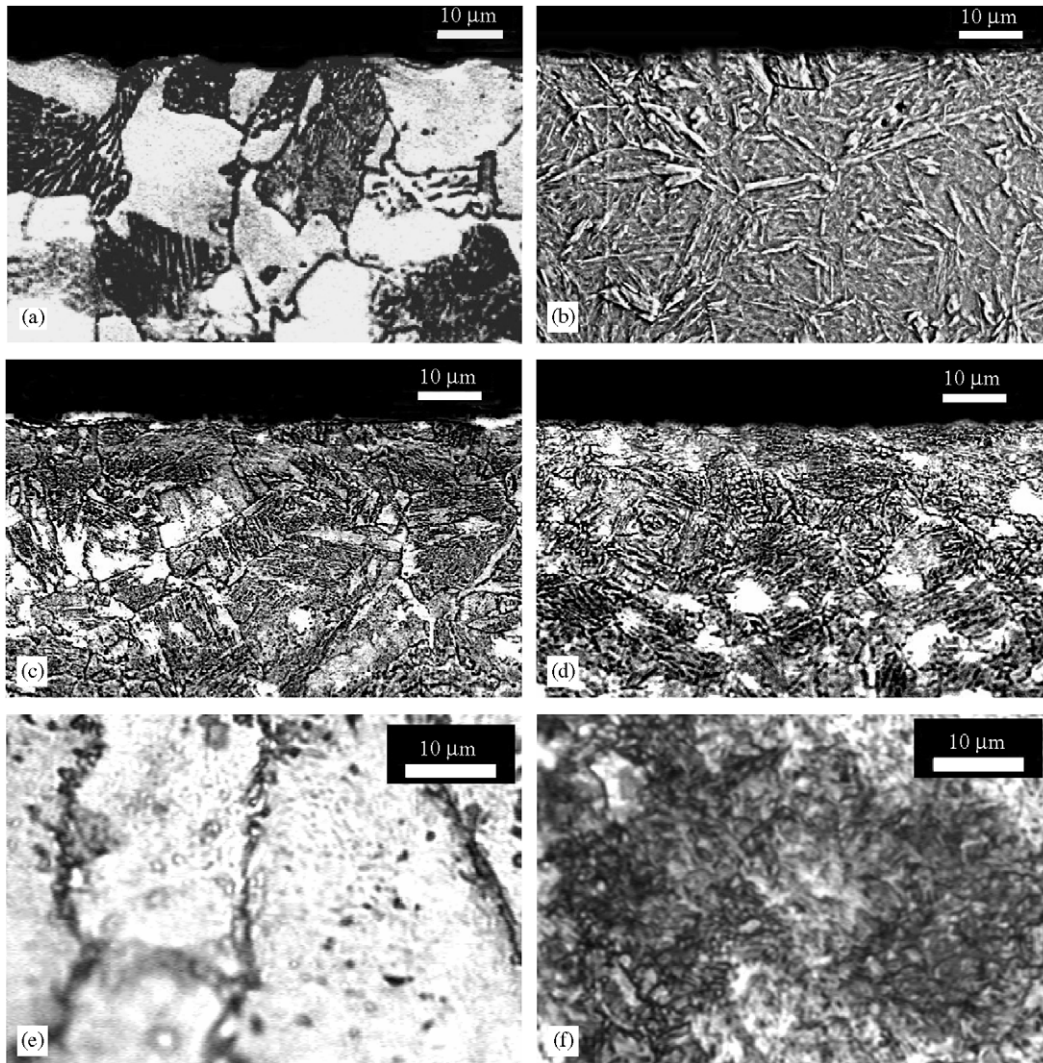


Fig. 5. The optical micrograph: (a) grinding with coolant; (b) heat treatment; (c–d) upper part of the GIL after grinding; (c) in the dry air; (d) with liquid nitrogen; (e–f) bottom of the GIL after grinding; (e) in the dry air; (f) with liquid nitrogen.

0.25 μm , confirming a ductile mode of material removal. The surface was shining and without oxidation (Fig. 3(a)). In contrast, the ground surface obtained in dry air appeared with dark colour. The EDX spectrum showed the oxygen peak (Fig. 3(b)), indicating a surface oxidation. In this case, the R_a roughness was 0.98 μm and it is clear that the lack of lubrication in grinding had led to discontinuous grooves (Fig. 2(b)). By examining the surfaces, it was found that spherical particles appeared on the surfaces ground in dry air, which were the melted grinding chips [17]. It is clear that the ground surface quality was further degraded by the ‘back-transfer’ of the workpiece metal [18].

On the contrary, the surfaces ground with liquid nitrogen were always shining, smooth and without any sign of oxidation or burning (Figs. 2(c) and 3(c)). These indicate that oxidation was suppressed. Therefore, it can be concluded that liquid nitrogen has successfully acted as a protective shielding in grinding.

3.2. Microstructure by optical microscopy

The optical micrographs of subsurface areas after grinding with different coolants are presented in Figs. 4 and 5.

No grinding-induced layers (GILs) were admitted with the application of Noritake coolant (Fig. 4(a)). The structure of material was composed of pearlite, arranged in the background of ferrite (Fig. 5(a)).

However, the GILs were found in both the components ground in dry air or with liquid nitrogen (Figs. 4(b and c)). The GIL in a specimen ground in dry air had a variable microstructure of martensite (Fig. 5(c)) and a depth of 350 μm . The martensite of the layer had a finer structure when compared with a plate-like laths martensite generated by an ordinary heat treatment (Fig. 5(b)). At the bottom of the GIL, it was found that there existed numerous ferrite grains with carbides precipitated along its boundaries (Fig. 5(e)).

The GIL in the specimen ground with liquid nitrogen was thinner, 85 μm in depth, but its structure was more even featuring martensite at the layer's bottom (Fig. 5(e)). Martensite of the GIL near the surface was optically undistinguishable from the GIL after grinding in dry air (Figs. 5(c and d)). (The difference can be revealed by electron microscopy, but this will be discussed in Section 3.4.)

3.3. Micro-hardness

The micro-hardness across the thickness of a GIL can be seen in Fig. 4. It is clear that a specimen's micro-hardness remained unchanged ($\text{HV}_{(500\text{g})} = 200$) (Fig. 4(a)) after the grinding with Noritake coolant. However, the micro-hardness of the GIL due to the grinding in dry air increased to $\text{HV}_{(500\text{g})} = 750$ (Fig. 4(b)), which is 3.75 times higher than that of the original steel and 1.15 times that of the ordinary martensite ($\text{HV}_{(500\text{g})} = 650$). There was a fluctuation of the micro-hardness across the GIL, which decreased to $\text{HV}_{(500\text{g})} = 400$ at the layer's bottom, because the microstructure changed to the ferrite–carbide arrangement. It was very promising that the micro-hardness of the GIL generated by the grinding with liquid nitrogen was even higher, $\text{HV}_{(500\text{g})} = 1100$ (Fig. 4(c)), which is 1.46 times higher than that of the GIL developed by the grinding in dry air. Furthermore, the micro-hardness decreased only slightly across the GIL thickness, which was still $\text{HV}_{(500\text{g})} = 700$ at the layer's bottom due to even martensite structure (Fig. 5(e)).

3.4. Microstructure revealed by electron microscopy

The microstructure of the upper part of the GIL (near the specimen's surface) induced by the grinding in dry air is shown in Fig. 6(a). The martensite laths are grouped in packets. The martensite crystals inside a packet are elongated in approximately the same direction, with an average length of 2–4 μm and an average width of 0.3–0.5 μm . The dislocation density is high. Dispersed precipitations with characteristic dimension of 20–50 nm were easily located at boundaries (Fig. 7(a)) and inside the laths (Fig. 7(c)). A diffraction analysis showed that they are interstitial carbides of two types, ξ -carbide $\text{Fe}_{2.4}\text{C}$ with hexagonal structure or η -carbide Fe_2C with orthorhombic structure [19]. Figs. 7(a and b) present the bright and dark images of ξ -carbide and diffraction pattern with zone axis $[\bar{1}\bar{1}1]$ of $\text{Fe}_{2.4}\text{C} \parallel$ to $[111]$ of martensite. η -carbide is presented in Figs. 7(c and d), with zone axis $[\bar{1}1\bar{1}]$ of $\text{Fe}_2\text{C} \parallel$ to $[331]$ of martensite.

The upper part of the GIL obtained with liquid nitrogen was composed of fine and nearly circular grains with a characteristic dimension of 0.2–0.3 μm . Moreover, the dislocation structure of the martensite fragments was mainly cellular, although polygonal regions occasionally appeared (Fig. 6(b)). No carbides were observed.

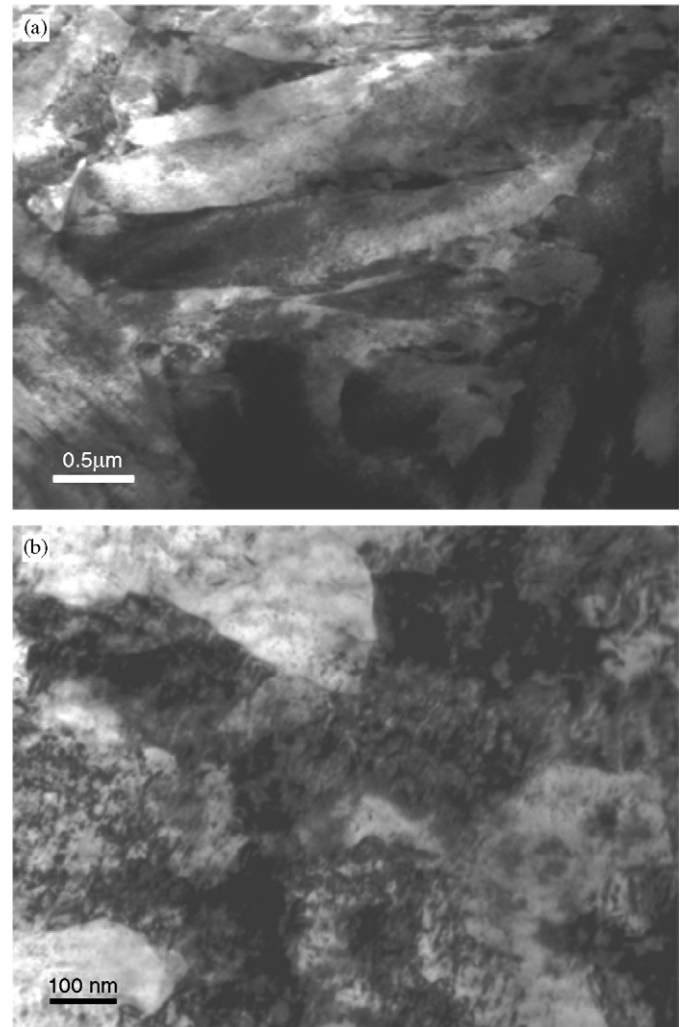


Fig. 6. The electron micrograph after grinding: (a) in the dry air; (b) with liquid nitrogen.

3.5. Residual stresses

The distributions of residual stresses in subsurface of ground components are shown in Fig. 4. In this figure, σ_{xx} and σ_{yy} are residual stresses measured along and perpendicular to the grinding direction, respectively.

Grinding with Noritake coolant produces compressive residual stresses of 200–400 MPa to the depth of 100 μm in the ground component for both measured directions (Fig. 4(a)).

On the contrary, grinding in dry air created tensile residual stresses of 100–200 MPa along the whole depth of the GIL (400 μm) in both xx and yy directions (Fig. 4(b)), which is not desirable in engineering applications because tensile surface residual stresses facilitate fracture, fatigue failure, corrosion and wear.

The application of liquid nitrogen created compressive residual stresses of 200 MPa, spreading to the depth of 85 μm (Fig. 4(c)), which is similar to those produced by the grinding with coolant. The origin of these advantages will be discussed below.

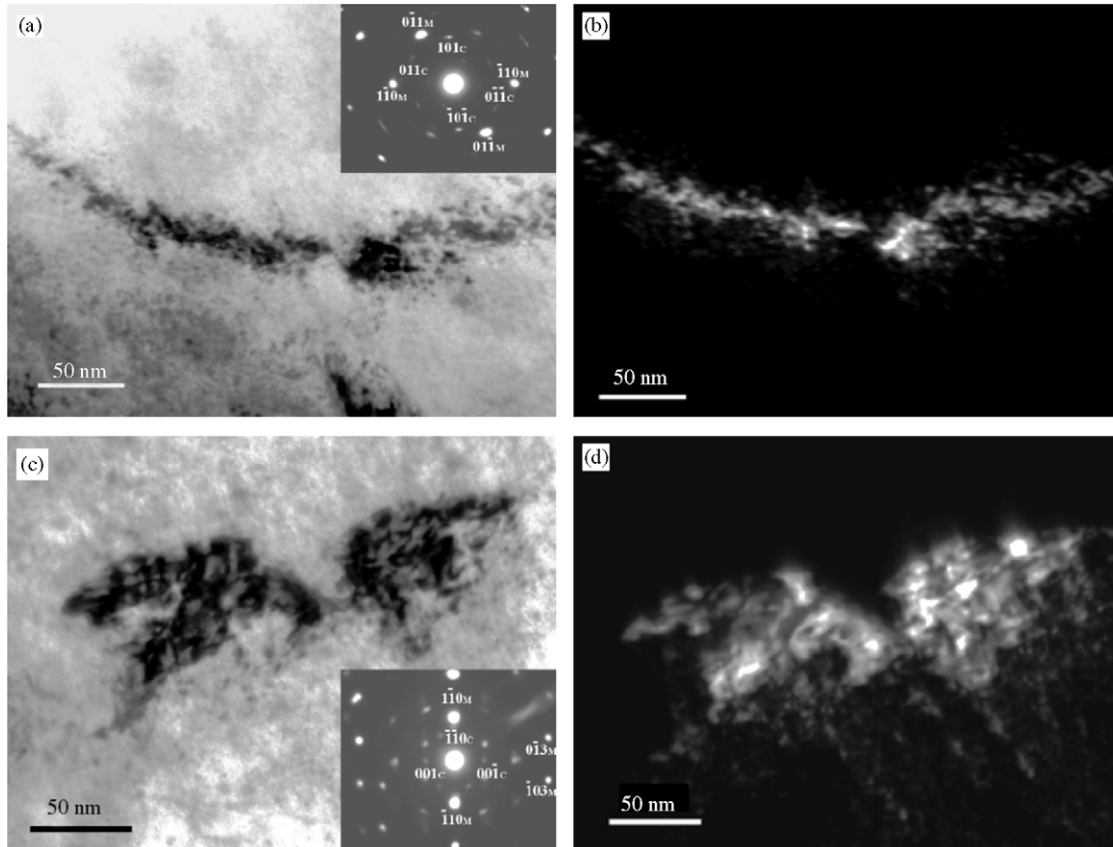


Fig. 7. The electron micrograph of interstitial carbides after grinding in the dry air: (a) the bright field and the indexed diffraction pattern (Note ϵ -carbides at laths boundary); (b) the dark field in the 101 $\text{Fe}_{2.4}\text{C}$ reflection; (c) the bright field and the indexed diffraction pattern (Note η -carbides inside martensite laths); (d) the dark field in the 001 Fe_2C reflection.

3.6. Mechanisms of heating, microstructure and residual stress development

The above results show that liquid nitrogen is a superior cooling medium for a grinding-hardening operation. Its application not only enhances the mechanical properties of a ground component and creates compressive residual stresses, but also eliminates surface oxidation. To achieve a deeper understanding, it is necessary to look into the heating mechanism that took place within the wheel-workpiece interaction zone and the development of the GIL microstructure and residual stresses during grinding.

In a grinding-hardening process, the development of the GIL is the result of phase transformations during which the steel is heated above A_{c3} . As the thickness of a martensite layer is known, which can be measured from Fig. 4, the surface temperature in grinding can be approximately estimated by [17]

$$\frac{A_{c3}}{\theta_s} = 1 - \text{erf} \left\{ y / \left[2 \left(\frac{k}{\rho C} \frac{(Dd)^{1/2}}{v_w} \right)^{1/2} \right] \right\},$$

where A_{c3} is the austenite transition temperature which is 795 °C for the 1045 steel used in this study, y is the

thickness of the martensitic layer, erf is the Gaussian error function, $k/\rho C$ is the thermal diffusivity, D is the wheel diameter, d is the depth of cut and v_w is the table speed. This formula predicts that the mean surface temperature, θ_s , should be 833 and 1023 °C, for grinding with liquid nitrogen and dry air, respectively. While such a high temperature rise in dry air is not surprising, the following discussion and experimental observation can explain how the large temperature rise occurred even with the application of liquid nitrogen whose boiling temperature is -196 °C.

It is well known that heating in grinding is localised within a very small grinding zone and the degree of grinding-heating depends on the quantity of the cooling medium penetrated into the zone [20]. As illustrated in Fig. 8(a), when liquid nitrogen is applied, its high evaporation rate is further raised by the turbulent air flow generated by wheel rotation. As a result, the penetration of liquid nitrogen into the grinding zone is extremely limited, leaving the wheel pores and workpiece in contact with only a little amount of nitrogen gas, as illustrated in the figure. Heat dissipation due to the boiling of liquid nitrogen is effective only in the vicinity of the grinding zone. Hence, a high temperature rise takes place inside the grinding zone. This mechanism is well demonstrated by the experiment

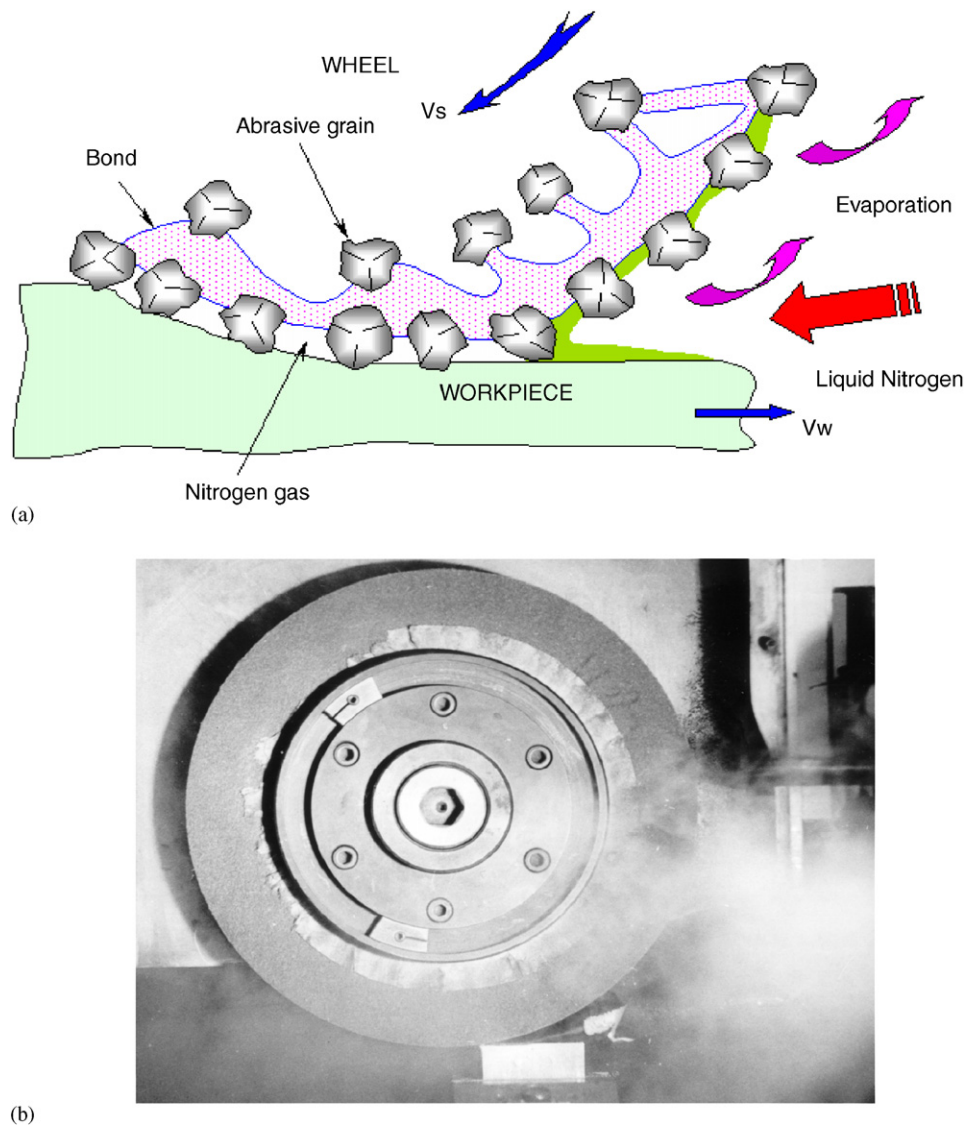


Fig. 8. Nitrogen penetration in the grinding zone: (a) schematic presentation; (b) general view (Note an extensive evaporation of nitrogen).

shown in Fig. 8(b), where significant amount of liquid nitrogen vapour appeared.

Now let us consider the microstructure development in grinding–hardening. As mentioned before, to initiate the GIL, it is necessary to bring the temperature above A_{c3} . According to our estimation previously, the grinding with liquid nitrogen met the condition. Moreover, the application of liquid nitrogen increased the cooling rate, so that the heat treatment cycle became different from the grinding in air or coolant (Fig. 9). Hence, the deformation of austenite during the grinding with liquid nitrogen occurred at a lower temperature and promoted the development of cellular and polygonal dislocation structures. The substructure generated in the austenite prevented the growth of martensite crystals, facilitated an increase in the number of nucleation centres, and caused the overall refinement of the martensite structure. Because of that, the martensite induced by the grinding with liquid nitrogen had a much finer structure (Fig. 6(b)).

The change in the cooling rate also affected the final GIL structure. The nose of the Bs curve in the TTT diagram of 1045 carbon steel is located at 540°C and is at 1 s [21]. It means that to avoid carbide precipitation the cooling rate must be above 500 grad/s for the grinding in dry air and 250 grad/s for that in liquid nitrogen. As the dry air-grinding failed to meet the condition, carbides were easily formed in the GIL (Fig. 7). Furthermore, the high strain rate in grinding changed the kinetics of their precipitation and endorsed the development of interstitial ϵ and η carbides. In the grinding with liquid nitrogen, however, the cooling rate was well above 250 grad/s. Hence, no carbides appeared.

Clearly, the GIL created by the grinding with liquid nitrogen is very advantageous due to the refinement of martensite and absence of carbides—both increase the hardness of the GIL.

Now let us consider the development of residual stresses. Relevant studies on residual stresses in a ground

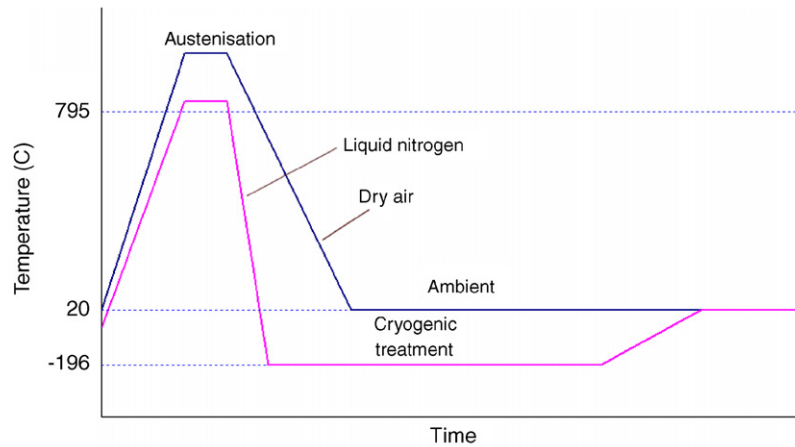


Fig. 9. Thermal cycles in grinding.

component have concluded that their creation is due to mechanical traction, thermal deformation and phase transformation [22]. The mechanical traction generally produces compressive stresses. The thermal deformation, however, often leads to tensile stresses. When phase transformation occurs, additional residual stresses appear, which can alter the resultant stress distribution [9,23,24]—either tensile or compressive, depending on the volume changes of the new phases. In the case of martensite transformation, compressive residual stresses arise as its body-centered tetragonal (BCT) lattice occupies more space than the original body-centered cubic (BCC) lattice of ferrite accomplished with orthorhombic lattice of cementite [21].

The tensile stresses generated by the grinding with dry air were due to the development of high heat (the temperature rise was 1023 °C as calculated before). At the same time, the precipitation of interstitial carbides Fe_2C and $Fe_{2.4}C$ lowered the volume of BCT martensite lattice and reduced the compressive stresses caused by phase transformation, leading to tensile resultant stresses.

In the grinding with liquid nitrogen, the smaller temperature rise (833 °C), fine homogeneous martensite structure (absence of carbides), and high mechanical traction all contributed to the generation of compressive resultant residual stresses.

4. Conclusions

This paper has presented an innovative development of a steel grinding–hardening technology using liquid nitrogen. The major conclusions are as follows:

1. The treatment can produce satisfactory surface integrity, including the compressive surface residual stresses and oxidation-free surface finish.
2. The phase transformations took place during grinding resulted in a martensite layer in a ground component.

The layer had a fine martensite structure which gives rise to a remarkably high hardness.

3. The grinding with liquid nitrogen is environmentally conscious.

References

- [1] E. Brinksmeier, T. Brockhoff, Utilization of grinding heat as a new heat treatment process, *Annals of the CIRP* 45 (1996) 283–286.
- [2] T. Brockhoff, Grind-hardening: a comprehensive view, *Annals of the CIRP* 48 (1999) 255–260.
- [3] S. Malkin, Burning limit for surface and cylindrical grinding of steels, *Annals of the CIRP* 27 (1978) 233–236.
- [4] M.C. Shaw, A. Vyas, Heat-affected zones in grinding steel, *Annals of the CIRP* 43 (1994) 279–282.
- [5] I. Zarudi, L.C. Zhang, A revisit to some wheel–workpiece interaction problems in surface grinding, *International Journal of Machine Tools and Manufacture* 42 (8) (2002) 905–913.
- [6] I. Zarudi, L.C. Zhang, Mechanical property improvement of quenchable steel by grinding, *Journal of Materials Science* 37 (18) (2002) 3935–3943.
- [7] I. Zarudi, L.C. Zhang, Modelling the structure changes in quenchable steel subjected to grinding, *Journal of Materials Science* 37 (2) (2002) 4333–4341.
- [8] M. Mahdi, L.C. Zhang, Applied mechanics in grinding, part VII: residual stresses induced by the full coupling of mechanical deformation, thermal deformation and phase transformation, *International Journal of Machine Tools & Manufacture* 39 (1999) 1285–1298.
- [9] M. Mahdi, L. Zhang, Applied mechanics in grinding—VI. Residual stresses and surface hardening by coupled thermo-plasticity and phase transformation, *International Journal of Machine Tools & Manufacture* 38 (1998) 1289–1304.
- [10] G.E. Linnert, *Welding Metallurgy, Carbon and Alloy Steel*, vol 1, American welding society, Miami, FL, USA, 1994.
- [11] P. Cohen, D. Kamody, Cryogenics goes deeper, *Cutting Tool Engineering* 50 (1998) 1–3.
- [12] P. Gorden, C.M., The transformation of retained austenite in high speed steel at subatmospheric temperatures, *Transactions of American Society for Metals* 30 (1942) 569–591.
- [13] J.R. Kennedy, A study of subzero treatments applied to Molybdenum–Tungsten high speed steel, *Transactions of American Society for Metals* 34 (1945) 251–309.

- [14] F. Meng, K. Tagashira, R. Azuma, Role of Eta-carbide precipitation in the wear resistance improvements of Fe–12Cr–Mo–V–1.4C tool steel by cryogenic treatment, *ISIJ International* 34 (1994) 205–210.
- [15] E.S. Zmud, Improved tool life after shock cooling, *Metals Science and Heat Treatment* 10 (1980) 701–703.
- [16] K. Nagai, T. Yuri, T. Ogata, O. Umezawa, K. Ishikawa, T. Nishimura, Cryogenic mechanical properties of Ti–6Al–4V alloys with three levels of oxygen content, *ISIJ International* 31 (1991) 882–889.
- [17] M.C. Shaw, *Principles of Abrasive Processing*, University Press, Oxford, 1996, pp. 574.
- [18] S. Malkin, *Grinding Technology—Theory and Applications of Machining with Abrasives*, EllisHorwood Ltd, Chichester, 1989, pp. 275.
- [19] A. Koniger, C. Hammerl, M. Zeitler, B. Rauschenbach, Formation of metastable iron carbide phases after high-fluence carbon ions implantation into iron at low temperatures, *Physical Review B* 55 (13) (1997) 8143–8147.
- [20] A.S. Lavine, T.C. Jen, Thermal aspects of grinding: heat transfer to workpiece, wheel, and fluid, *Transactions of the ASME* 113 (1991) 296–303.
- [21] G. Krauss, *Steels: Principles of Heat Treatment of Steels*, ASM International, Metals Park, OH, 1980.
- [22] L.C. Zhang, T. Suto, H. Noguchi, T. Waida, A study of creep-feed grinding of metallic and ceramic materials, *Journal of Materials Processing Technology* 48 (1995) 267–274.
- [23] L.C. Zhang, T. Suto, H. Noguchi, T. Waida, An overview of applied mechanics in grinding, *Manufacturing Review* 5 (1992) 261–273.
- [24] M. Mahdi, L.C. Zhang, Applied mechanics in grinding-V. Thermal residual stresses, *International Journal of Machine Tools & Manufacture* 37 (1997) 619–633.